

Available online at www.sciencedirect.com

Solar Energy xxx (2007) xxx–xxx

**SOLAR
ENERGY**
www.elsevier.com/locate/solener

2 Modeling of the optimum tilt of a solar chimney for maximum air flow

3 E.P. Sakonidou^{a,b}, T.D. Karapantsios^{b,*}, A.I. Balouktsis^a, D. Chassapis^a

4 ^a Department of Mechanical Engineering, Technological Educational Institution of Serres, End of Magnesia's Str, GR-62100 Serres, Greece

5 ^b Division of Chemical Technology, Department of Chemistry, Aristotle University of Thessaloniki, University Box 116, GR-54124 Thessaloniki, Greece

6 Received 18 July 2006; received in revised form 5 February 2007; accepted 6 March 2007

8 Communicated by: Associate Editor S.A. Sherif

9 Abstract

10 The aim of this work is to develop a mathematical model to determine the tilt that maximizes natural air flow inside a solar chimney
 11 using daily solar irradiance data on a horizontal plane at a site. The model starts by calculating the hourly solar irradiation components
 12 (direct, diffuse, ground-reflected) absorbed by the solar chimney of varying tilt and height for a given time (day of the year, hour) and
 13 place (latitude). In doing so it computes the transmittance and absorbance of the glazing for the various solar irradiation components
 14 and for various tilts. The model predicts the temperature and velocity of the air inside the chimney as well as the temperatures of the
 15 glazing and the black painted absorber. Comparisons of the model predictions with CFD calculations delineate the usefulness of the
 16 model. In addition, there is a good agreement between theoretical predictions and experiments performed with a 1 m long solar chimney
 17 at different tilt positions.

18 © 2007 Published by Elsevier Ltd.

19 *Keywords:* Solar chimney; Chimney effect; Natural ventilation; Solar air heater; Tilt; Maximum flow

21 1. Introduction

22 Solar chimneys differ from conventional chimneys in
 23 that their southern wall (for the north hemisphere) is
 24 replaced by a transparent sheet, i.e. glazing, that allows
 25 the collection and use of solar irradiation. Many works,
 26 especially the last two decades, have illustrated the advan-
 27 tages in using solar chimneys accounting also for their low
 28 maintenance cost and superb durability. Solar chimneys
 29 have been traditionally used in agriculture for air renewal
 30 in barns, silos, greenhouses, etc. as well as in drying of
 31 crops, grains, fruits or wood (e.g. Garg, 1987; Das and
 32 Kumar, 1989; Ekechukwu and Norton, 1995; Vlachos
 33 et al., 2002). Another popular application is for natural
 34 ventilation in buildings in order to improve the quality of
 35 indoors air and increase the comfort index for inhabitants

(e.g. Kumar et al., 1998; Ziskind et al., 2002; Ding et al., 36
 2004; Bansal et al., 2005). Having in mind climatization 37
 and energy conservation in buildings, efforts have also been 38
 made to evaluate the performance of special chimney con- 39
 figurations, such as solar roof collectors and Trombe-walls 40
 (e.g. Gan, 1998; Sánchez et al., 2003; Ong and Chow, 2003; 41
 Khedari et al., 2000, 2003; Heras et al., 2005) as well as 42
 other hybrid constructions involving inclined, vertical or 43
 horizontal heated walls with cooling cavities (e.g. Raman 44
 et al., 2001; Jiang and Chen, 2003; Kazansky et al., 2003; 45
 Dai et al., 2003). 46

Most published works deal with solar chimneys fixed at 47
 a specific inclination, usually vertical, as these are easier to 48
 construct and operate. To overcome the diurnal variability 49
 of solar irradiance, some of them used heating elements to 50
 maintain either uniform wall temperature or wall heat flux 51
 and examined only the heat transfer and fluid mechanics 52
 performance of the chimney (e.g. Bouchair and Fitzgerald, 53
 1988; Bouchair, 1994; Moshfegh and Sandberg, 1999; 54
 Afonso and Oliveira, 2000; Chen et al., 2003). These studies 55

* Corresponding author. Tel.: +30 2310997772; fax: +30 2310997759.
 E-mail address: karapant@chem.auth.gr (T.D. Karapantsios).

Nomenclature

Latin symbols

a	absorptance
A	surface area
C_d	discharge coefficient
c_p	specific heat
d	depth of the chimney gap
D_H	hydraulic diameter of the chimney
f	wall friction coefficient
G_{sc}	solar constant (1367 W/m ²)
h	convective heat transfer coefficient
hour	hour of the day
H	daily irradiation on a horizontal plane
H_{ch}	height difference between outlet and inlet of the chimney
H_0	daily extraterrestrial irradiation on a horizontal plane
I	hourly irradiation on a horizontal plane
K	extinction coefficient of the glass
k_{in} and k_{out}	inlet and outlet pressure loss coefficients
k_T	clearness index
ℓ	path length of irradiation through the glass
L	length of the chimney
n	day of the year (1 to 365)
Nu	Nusselt number
r	ratio of the hourly irradiation over the daily irradiation
r_g	diffuse reflectance of the surroundings
r_{\perp}	perpendicular component of unpolarized irradiation
r_{\parallel}	parallel component of unpolarized irradiation
R_b	ratio of the direct irradiation on a tilted plane over that on the horizontal plane
Ra	Rayleigh number
Ra_c	critical Rayleigh number
Re	apparent Reynolds number
s	slope of the chimney with respect to the horizontal plane
T	temperature

U	overall heat transfer coefficient
w	width of the chimney gap

Greek symbols

α and β	coefficients in Eq. (9)
δ	declination (angular position of the sun at solar noon)
ε	emittance of the black wall
η_1 and η_2	refraction indexes of air and glass, respectively
θ	angle
θ_1	angle of irradiation incidence
θ_2	angle of refraction
λ	thermal conductivity of air
μ	viscosity
ρ	density
σ	Stefan-Boltzmann constant ($= 5.6697 \times 10^{-8}$ W/m ² K ⁴)
τ	glass transmittance,
τ_r	average of r_{\perp} and r_{\parallel}
v	average air velocity inside the chimney
ϕ	latitude of the site (angular distance from the equator)
ω	hour angle

Subscripts

α	absorber
abs	absorption
air	air
bw	black wall
dif	diffuse
dir	direct
g	glazing
gap	chimney gap
0	ambient conditions
ref	reflection
s	sunset
T	tilted plane

56 showed that there are distinctly different flow patterns
57 between narrow and wide chimney gaps and that the ratio
58 of chimney length/gap influences the air flow rate.

59 Awbi and Gan (1992) obtained analytically the air tem-
60 perature and flow rate profiles along a Trombe wall, con-
61 sidering a uniform wall temperature. The same authors
62 employed also CFD codes to simulate the air flow and heat
63 transfer in a chimney of varying gap width (for large gaps
64 3D simulations were indispensable). Both analytical and
65 numerical results were in good agreement with earlier data.
66 Bansal et al. (1993) developed a steady state analytical
67 model for uniform wall temperature applied to a solar sys-
68 tem consisting of a solar air heater connected to a conven-
69 tional chimney. Andersen (1995) derived a set of equations

to predict the natural ventilation in a room with small 70
openings based on the pressure model. Gan (1998) and 71
Gan and Riffat (1998) used 3D CFD techniques to study 72
the parameters that influence the performance of a Trombe 73
wall. An interesting result of these studies was that ventila- 74
tion rates increased along with the thickness of the interior 75
wall. Moshfegh and Sandberg (1999), investigated air 76
movement behind photovoltaic panels using a 2D CFD 77
code coupled with a standard k - ε turbulence model and a 78
wall function. Their predictions of air velocity and temper- 79
ature distributions were in accord with their experimental 80
results. A similar 2D CFD approach was also adopted by 81
Rodrigues et al. (2000) who provided detailed calculations 82
of the velocity and temperature profiles in the chimney. 83

84 Using the concept of a thermal resistance network, Ong
85 and Chow (2003) developed an analytical model to exam-
86 ine the effects of air gap and solar irradiation intensity on
87 the performance of different chimneys assuming uniform
88 heat flux on the heated wall. Many of the above studies
89 provided evidence that for chimneys with gap-to-length
90 ratio less than or close to 1:10, the temperature can be
91 assumed uniform across the chimney gap and so 2D mod-
92 els can give reasonably accurate predictions.

93 Solar chimneys employing inclined collectors can evi-
94 dently exploit more the incident irradiation to enhance
95 air flow in the chimney. As the inclination of the chimney
96 varies, two things occur that work in opposite directions
97 with respect to the air flow rate. A higher inclination results
98 in a higher exposure of the wall to solar irradiation and
99 hence yield higher heat utilization and more intense buoy-
100 ant airflow. On the other hand, tilting the chimney reduces
101 the effective pressure head of the chimney and so dimin-
102 ishes air flow. It is apparent that there must be an optimum
103 tilt that leads to the highest flow rate, compromising these
104 two effects. Although there are a few studies coping with
105 the effect of inclination on a chimney performance, they
106 usually involve heating means other than solar irradiance
107 to achieve uniform wall heat flux (e.g. Moshfegh and Sand-
108 berg, 1999; Chen et al., 2003) and so a parametric analysis
109 with respect to the temporal variability of solar irradiation
110 is not possible.

111 To our knowledge, there are only two earlier studies that
112 examined systematically the effect of inclination for chim-
113 neys where the absorbed heat flux depends on the diurnal
114 and seasonal variations of solar irradiation. The first is
115 the work by Prasad and Chandra (1990) who performed
116 numerical calculations and also did experiments for a solar
117 chimney 1.5 m long and with 20 mm gap width. Their
118 model, though detailed for the momentum and heat trans-
119 fer in the fluid, had certain drawbacks: did not account for
120 heat losses, required knowledge of the ratio of diffuse/total
121 irradiation and, finally, assumed that the transmittance of
122 the glazing and absorptance of the black wall were unity
123 although it is known that these quantities vary with inclina-
124 tion (Duffie and Beckman, 1991). The agreement between
125 predictions and experiments was rather poor but their find-
126 ing that the optimum tilt for maximum irradiance uptake
127 (i.e. maximum air temperature), is distinctly different than
128 the optimum tilt for maximum air velocity in the chimney
129 was significant. They calculated optimum tilt angles for
130 maximum air velocity to oscillate periodically throughout
131 the year between a low value, 52°, in summer months
132 and a high value, 72°, in winter months (for Calcutta,
133 India). A much simpler treatment of solar irradiation and
134 glazing optical properties was employed by Hamdy and
135 Fikry (1998) for Alexandria (Egypt) and summer months.
136 For these particular conditions, an optimum tilt around
137 60° was estimated for maximum air flow.

138 Data of solar irradiation at a site that are easily accessi-
139 ble by a design engineer usually refer to monthly average
140 daily values of total irradiation on a horizontal plane,

e.g. ELOT (1991). Therefore for designing a solar chimney, 141
horizontal irradiation data have first to be transformed to 142
irradiation data at a slope. For accurate estimations, it is 143
important to base the design on hourly values of solar irra- 144
diation which must then be determined from the available 145
daily values. In any case, it is necessary to decompose the 146
total irradiation arriving at the sloped surface into its 147
major components (direct, diffuse and ground-reflected) 148
since for each of them the optical properties (transmittance 149
and absorptance) of the glass cover varies differently with 150
the tilt. As far as we know, there is no prior work that deals 151
with the estimation of the optimum tilt of a solar chimney 152
for maximizing air flow starting from data of daily total 153
solar irradiation on an horizontal plane and taking into 154
account all the above considerations. It is indeed the scope 155
of this study to propose an engineering model that can 156
cope with this task. The term engineering denotes a simpli- 157
fied model adequate for design purposes and field applica- 158
tions which does not employ detailed 2D/3D fluid 159
mechanics and heat transfer calculations. 160

161 In the following, the setup of the engineering and CFD
162 models is presented first. Next, the solar chimney construc-
163 tion and operation are outlined. Finally, theoretical predic-
164 tions from the models are compared and discussed against
165 each other and against experimental results.

2. Theory 166

2.1. Engineering model 167

168 In the analysis below, it is assumed that the incident
169 solar irradiation is sufficient to bring the chimney's body
170 to its steady state temperature. The input data to the model
171 are divided in five categories: (a) chronological (day of the
172 year, hour) and geographical (latitude), (b) meteorological
173 (monthly average daily total irradiation on an horizontal
174 plane, monthly average daily ambient temperature), (c)
175 geometrical (dimensions of chimney, thicknesses of glazing
176 and insulation material), (d) optical/irradiation properties
177 of the construction materials (refractive index and extinc-
178 tion coefficient of the glazing, absorptance and emittance
179 of the black surfaces), and (e) physical properties of air and
180 insulation materials for calculating heat losses). The chim-
181 ney tilt and length are treated as variables in the range
182 30–90° (angles from the horizontal plane) and 1–12 m,
183 respectively. Physical properties of air are taken from
184 VDI-Wärmeatlas (1991). Data for monthly average daily
185 total irradiation and monthly average ambient temperature
186 are taken from ELOT (1991) – the Greek Organization of
187 Standardization – for Serres, a city in North Greece where
188 also the experimental tests are performed. The ELOT data
189 agree reasonably well with measurements from the meteo-
190 rological station of TEI – Serres with only a ~3% annual
191 deviation (Karapantsios et al., 1999).

192 The model consists of three basic subroutines. The first
193 one estimates the solar irradiation components (direct,
194 diffuse and ground-reflected) that hit the surface of the

chimney on an hourly basis, at varying tilt and length. For this calculation, only the chronological, geographical and meteorological information mentioned above is needed. The relations below, unless differently stated, are taken from Duffie and Beckman (1991).

The total daily irradiation on a horizontal plane, H , is customary expressed as the sum of two components: the direct (beam) irradiation and the diffuse irradiation from the sky

$$H = H_{\text{dir}} + H_{\text{dif}} \quad (1)$$

The daily extraterrestrial solar irradiation H_0 on a horizontal plane is given as

$$H_0 = \frac{24 \times 3600}{\pi} G_{\text{sc}} \left(1 + 0.033 \cos \frac{360n}{365} \right) \times \left[\cos \phi \cos \delta \sin \omega_s + \frac{\pi \omega_s}{180} \sin \phi \sin \delta \right] \quad (2)$$

where G_{sc} is the solar constant (1367 W/m^2), n is the day of the year (1–365), ϕ is the latitude of the site (angular distance from the equator, for Serres ($\phi = 41$)), δ is the declination (angular position of the sun at solar noon) and ω_s is the sunset hour angle given as

$$\omega_s = \arccos(-\tan \phi \tan \delta) \quad (3)$$

The declination δ is found from the equation:

$$\delta = 23.45 \sin \left(360 \frac{284 + n}{365} \right) \quad (4)$$

The daily extraterrestrial solar irradiation H_0 is related with the daily total irradiation H (input variable to the code), via the clearness index k_T :

$$k_T = \frac{H}{H_0} \quad (5)$$

Knowing the value of the clearness index, one can calculate the diffuse component, H_{dif} , as follows for $\omega_s \leq 81.4^\circ$:

$$\frac{H_{\text{dif}}}{H} = \begin{cases} 1.0 - 0.2727k_T + 2.4495k_T^2 - 11.9514k_T^3 + 9.3879k_T^4 & \text{for } k_T < 0.715 \\ 0.143 & \text{for } k_T \geq 0.715 \end{cases} \quad (6)$$

whereas for $\omega_s > 81.4^\circ$

$$\frac{H_{\text{dif}}}{H} = \begin{cases} 1.0 + 0.2832k_T - 2.5557k_T^2 + 0.8448k_T^3 & \text{for } k_T < 0.722 \\ 0.143 & \text{for } k_T \geq 0.722 \end{cases} \quad (7)$$

Then, the direct daily component can be computed from Eq. (1). The ratio of the total hourly irradiation, I , over the total daily irradiation, H , is given by

$$r_t = \frac{I}{H} \quad (8)$$

and can be found from the relation

$$r_t = \frac{\pi}{24} (\alpha + \beta \cos \omega) \frac{\cos \omega - \cos \omega_s}{\sin \omega_s - \frac{\pi \omega_s}{180} \cos \omega_s} \quad (9)$$

where the coefficients α and β are given by 243

$$\alpha = 0.409 + 0.5016 \sin(\omega_s - 60) \quad (10)$$

$$\beta = 0.6609 - 0.4767 \sin(\omega_s - 60) \quad (11) \quad 245$$

and the hour angle ω that appears above is given by 246

$$\omega = (\text{hour} - 12) * \frac{360}{24} \quad (12) \quad 248$$

where *hour* denotes the hour of the day (input variable). 249

Likewise, the ratio of the hourly diffuse irradiation, I_{dif} , over the daily diffuse irradiation, H_{dif} , is given as 250 251 252

$$r_{\text{dif}} = \frac{I_{\text{dif}}}{H_{\text{dif}}} \quad (13) \quad 254$$

where 255

$$r_{\text{dif}} = \frac{\pi}{24} \frac{\cos \omega - \cos \omega_s}{\sin \omega_s - \frac{\pi \omega_s}{180} \cos \omega_s} \quad (14) \quad 257$$

Then, I and I_{dif} are calculated from Eqs. (8) and (13), respectively, whereas the hourly direct irradiation, I_{dir} , is computed as 258 259 260

$$I_{\text{dir}} = I - I_{\text{dif}} \quad (15) \quad 262$$

A customary approach for irradiation estimations on sloped surfaces is to consider an isotropic 2D model for the diffuse irradiation (Liu and Jordan, 1963) and also assume that the reflecting surfaces are diffuse and not specular reflectors. Recent studies, (e.g. Badescu, 2002) have shown that isotropic 3D models perform better than the Liu–Jordan isotropic 2D model which seems to overestimate the diffuse and underestimate the ground reflected solar irradiation component, respectively. For sites around our latitude or smaller, the diffuse and reflected components are usually much less than the direct solar irradiation component. In addition, for the most common chimneys inclinations (close to vertical) the differences between 2D and 3D models diminish and, therefore, can be safely ignored. For these reasons the present calculations utilize the well-known Liu–Jordan isotropic 2D model. In this case, the total irradiation on a surface tilted at slope s , is given by Sukhatme (1984) 263 264 265 266 267 268 269 270 271 272 273 274 275 276 277 278 279 280 281

$$I_T = I_{\text{dir}} R_b + I_{\text{dif}} \left(\frac{1 + \cos s}{2} \right) + I_r \left(\frac{1 - \cos s}{2} \right) \quad (16) \quad 283$$

On the RHS of Eq. (16), the first term represents the direct component, the second term the diffuse component and the third term the component that is reflected from the surroundings. In (16), r_g is the diffuse reflectance of the surroundings (usually around 0.25) and R_b is the ratio of direct irradiation on the tilted surface over that on the horizontal plane. R_b for the northern hemisphere is given by Sukhatme (1984): 284 285 286 287 288 289 290 291

$$R_b = \frac{\cos(\phi - s) \cos \delta \cos \omega + \sin(\phi - s) \sin \delta}{\cos \phi \cos \delta \cos \omega + \sin \phi \sin \delta} \quad (17) \quad 293$$

294 Thus, the average hourly irradiation components on a
295 tilted surface that enter in the calculations of the solar
296 chimney are

$$I_{T,\text{dir}} = I_{\text{dir}} \cdot R_b \quad (18)$$

$$I_{T,\text{dif}} = I_{\text{dif}} \cdot \left(\frac{1 + \cos s}{2} \right) \quad (19)$$

$$298 \quad I_{T,\text{ref}} = I \cdot 0.25 \cdot \left(\frac{1 - \cos s}{2} \right) \quad (20)$$

299 The second subroutine of the model evaluates the trans-
300 mittance, τ , and absorptance, a_g , of the glazing for the var-
301 ious components of the incident solar irradiation. The
302 transmittance for the direct irradiation component, τ_{dir} , is
303 approximately given by the product:

$$306 \quad \tau_{\text{dir}} \cong \tau_{zbs,\text{dir}} \cdot \tau_{\text{ref},\text{dir}} \quad (21)$$

307 where $\tau_{zbs,\text{dir}}$ denotes the ratio of the transmitted versus the
308 incident irradiation where only absorption losses have been
309 considered and $\tau_{\text{ref},\text{dir}}$ denotes the transmittance of initially
310 unpolarized irradiation where only reflection losses have
311 been considered.

312 In Eq. (21), $\tau_{zbs,\text{dir}}$ is given as

$$314 \quad \tau_{zbs,\text{dir}} = \exp \left(- \frac{K\ell}{\cos \theta_2} \right) \quad (22)$$

where K is the extinction coefficient of the glass that varies
315 from approximately 4 m^{-1} for “water white” glass to
316 approximately 32 m^{-1} for poor (greenish cast of edge) glass
317 (Duffie and Beckman, 1991). In this work, $K = 10 \text{ m}^{-1}$.
318 Moreover, ℓ designates the path length of irradiation
319 through the glass which in effect is the thickness of the
320 glass. In this work, $\ell = 0.004 \text{ m}$. Finally, θ_2 is the angle
321 of refraction, which is calculated from the expression:
322

$$\frac{\eta_1}{\eta_2} = \frac{\sin \theta_1}{\sin \theta_2} \quad (23) \quad 324$$

where η_1 and η_2 are the refraction indexes of air and glass,
325 respectively; in this work, $\eta_1 = 1$ and $\eta_2 = 1.526$ (Duffie
326 and Beckman, 1991). Furthermore, θ_1 is the angle of inci-
327 dence calculated as
328

$$\theta_1 = \arccos [\sin(\phi - s) \sin \delta + \cos(\phi - s) \cos \delta \cos \omega] \quad (24) \quad 331$$

The parameter τ_r is the average of two components
332

$$\tau_{r,\text{dir}} = \frac{1}{2} \left(\frac{1 - r_{\parallel}}{1 + r_{\parallel}} + \frac{1 - r_{\perp}}{1 + r_{\perp}} \right) \quad (25) \quad 334$$

where r_{\perp} represents the perpendicular component and r_{\parallel}
335 the parallel component of unpolarized irradiation given by
336

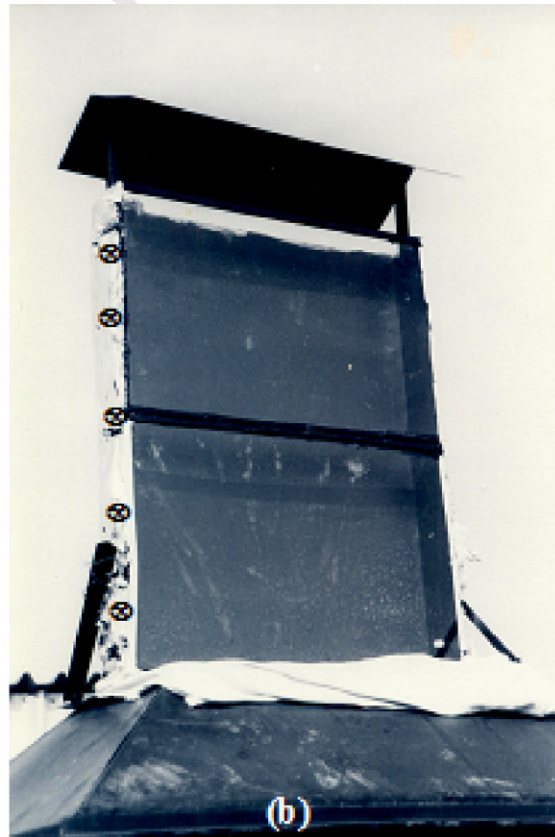
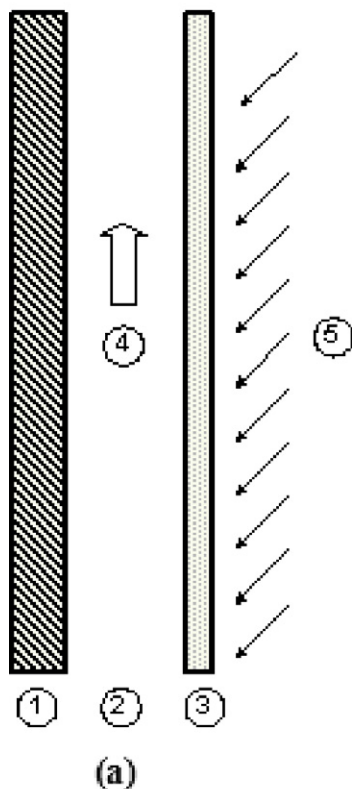


Fig. 1. Solar chimney configuration. (a) schematic of the cross-section of a solar chimney showing critical elements, 1: insulated black-painted absorber, 2: air entry, 3: glazing, 4: air flow direction, 5: incident irradiation and (b) photo of the chimney employed in the experiments (⊗: measuring station).

$$r_{\perp} = \frac{\sin^2(\theta_2 - \theta_1)}{\sin^2(\theta_2 + \theta_1)} \quad (26)$$

$$r_{\parallel} = \frac{\tan^2(\theta_2 - \theta_1)}{\tan^2(\theta_2 + \theta_1)} \quad (27)$$

The diffusion component, τ_{dif} , and the reflection component, τ_{ref} , of the glass transmittance, are calculated in the same manner as τ_{dir} but with the slope s in Eq. (24) replaced by the diffusion angle, θ_{dif} , and the reflection angle, θ_{ref} , respectively, defined as

$$\theta_{\text{dif}} = 59.7 - 0.1388 \cdot s + 0.001497 \cdot s^2 \quad (28)$$

and

$$\theta_{\text{ref}} = 90 - 0.5788 \cdot s + 0.002693 \cdot s^2 \quad (29)$$

Accordingly, the components of the glass absorptance: direct, $a_{\text{g,dir}}$, diffuse, $a_{\text{g,dif}}$ and reflected, $a_{\text{g,ref}}$, are given by the following approximate relations:

$$a_{\text{g,dir}} \cong 1 - \tau_{\text{zbs,dir}} \quad (30)$$

$$a_{\text{g,dif}} \cong 1 - \tau_{\text{zbs,dif}} \quad (31)$$

$$a_{\text{g,ref}} \cong 1 - \tau_{\text{zbs,ref}} \quad (32)$$

For conciseness, the products $(\tau \cdot I)_{\text{T}}$ and $(a_{\text{g}} \cdot I)_{\text{T}}$ will henceforth denote the following quantities:

$$(\tau \cdot I)_{\text{T}} = \tau_{\text{dir}} \cdot I_{\text{T,dir}} + \tau_{\text{dif}} \cdot I_{\text{T,dif}} + \tau_{\text{ref}} \cdot I_{\text{T,ref}} \quad (33)$$

$$(a_{\text{g}} \cdot I)_{\text{T}} = a_{\text{g,dir}} \cdot I_{\text{T,dir}} + a_{\text{g,dif}} \cdot I_{\text{T,dif}} + a_{\text{g,ref}} \cdot I_{\text{T,ref}} \quad (34)$$

These are quantities that appear in the heat balance equations of the chimney and therefore need be evaluated first when running the code.

The third subroutine of the model solves the overall energy balance of the chimney in the form of a system of three algebraic equations describing the heat exchange across the black wall (absorber), the glazing and the air inside the chimney, respectively. Fig. 1b shows a schematic representation of the solar chimney configuration including most critical elements. The heat exchange equations are (temperatures in Kelvin)

$$a_{\text{bw}}(\tau \cdot I)_{\text{T}} A_{\text{g}} = U_{\text{bw}} \cdot A_{\text{bw}} \cdot (T_{\text{bw}} - T_0) + h_{\text{bw}} \cdot A_{\text{bw}} \cdot (T_{\text{bw}} - T_{\text{air}}) + \varepsilon \cdot \sigma \cdot A_{\text{g}} \cdot (T_{\text{bw}}^4 - T_{\text{g}}^4) \quad (35)$$

$$(a_{\text{g}} \cdot I)_{\text{T}} A_{\text{g}} + \varepsilon \cdot \sigma \cdot A_{\text{g}} \cdot (T_{\text{bw}}^4 - T_{\text{g}}^4) = h_{\text{g}} \cdot A_{\text{g}} \cdot (T_{\text{g}} - T_{\text{air}}) + U_{\text{g}} \cdot A_{\text{g}} \cdot (T_{\text{g}} - T_0) \quad (36)$$

$$h_{\text{bw}} \cdot A_{\text{bw}} \cdot (T_{\text{g}} - T_{\text{air}}) + h_{\text{g}} \cdot A_{\text{g}} \cdot (T_{\text{g}} - T_{\text{air}}) = 2 \cdot c_{p,\text{air}} \cdot \rho_{\text{air}} \cdot A_{\text{gap}} \cdot v \cdot (T_{\text{air}} - T_0) \quad (37)$$

In these equations, the three unknowns are T_{bw} the average temperature of the black wall, T_{air} the average air temperature in the chimney and T_{g} the average glass temperature. T_0 , is the ambient temperature which is an input variable. Moreover, A_{bw} is the surface area of the black wall, A_{g} is the surface area of the glass cover and A_{gap} is the cross sectional area of the chimney gap. Furthermore, U_{bw} is the overall heat transfer coefficient between the black wall and the surroundings (in this work,

$U_{\text{bw}} = 0.9 \text{ W/m}^2 \text{ K}$ for a typical insulation thickness of 5 cm with thermal conductivity of 0.045 W/m K and moderate ambient conditions), U_{g} is the overall heat transfer coefficient between the glass cover and the surroundings (in this work, $U_{\text{g}} = 9 \text{ W/m}^2 \text{ K}$ chosen from the range $1\text{--}15 \text{ W/m}^2 \text{ K}$ proposed by Garg (1987), h_{bw} is the convective heat transfer coefficient between the black wall and the air in the chimney and h_{g} is the convective heat transfer coefficient between the glass cover and the air in the chimney. In addition, a_{bw} is the absorptance of the black wall (in this work, $a_{\text{bw}} = 0.9$, a value chosen from Duffie and Beckman (1991), ε is the emittance of the black wall (in this work, $\varepsilon = 0.95$, a value chosen from Duffie and Beckman (1991). Also, σ is the Stefan-Boltzmann constant ($= 5.6697 \times 10^{-8} \text{ W/m}^2 \text{ K}^4$) whereas $c_{p,\text{air}}$ and ρ_{air} are the temperature dependent specific heat and density of air, respectively. Finally, v is the average air velocity along the chimney which since it can not stand as a fourth unknown in the above system of equations it must be described by some relation based on the other parameters of the system (see below).

The convective heat transfer coefficients for both the glass cover and the black wall and strictly for the vertical position of the chimney are given by the relation (VDI-Wärmeatlas, 1991):

$$Nu_{\text{g,bw}} = \frac{h_{\text{g,bw}} L}{\lambda} = \left\{ 0.825 + 0.387 \cdot (0.345 \cdot Ra_{\text{g,bw}})^{1/6} \right\}^2 \quad (38)$$

for $10^{-1} < Ra \sin(s) < 10^{12}$

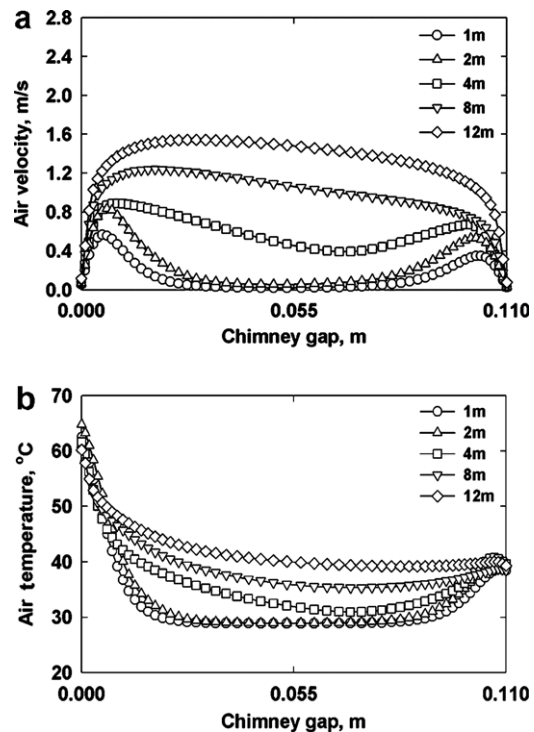


Fig. 2. Air velocity profile (a) and air temperature profile (b) across the chimney gap for different chimney lengths at the vertical position as calculated by the CFD model (day = 196, $H = 23.1 \text{ MJ/m}^2$, $T_{\text{amb}} = 28.9 \text{ }^\circ\text{C}$).

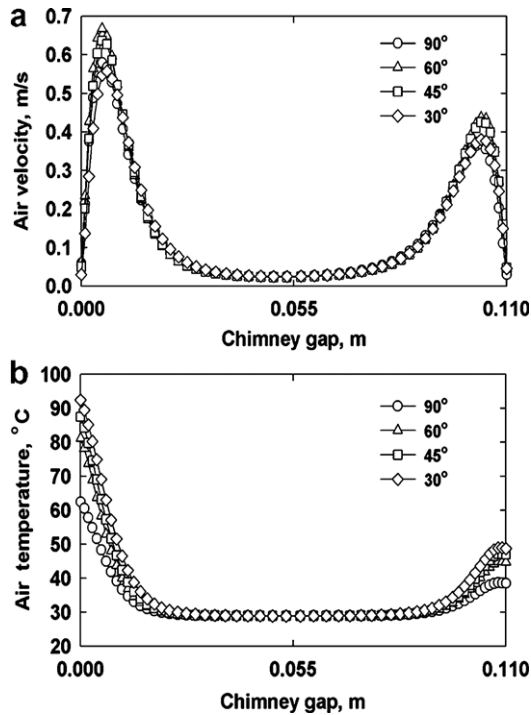


Fig. 3. Air velocity profile (a) and air temperature profile (b), across the chimney gap for different tilt angles for a chimney of 1m length as calculated by the CFD model (day = 196, $H = 23.1 \text{ MJ/m}^2$, $T_{\text{amb}} = 28.9 \text{ }^\circ\text{C}$).

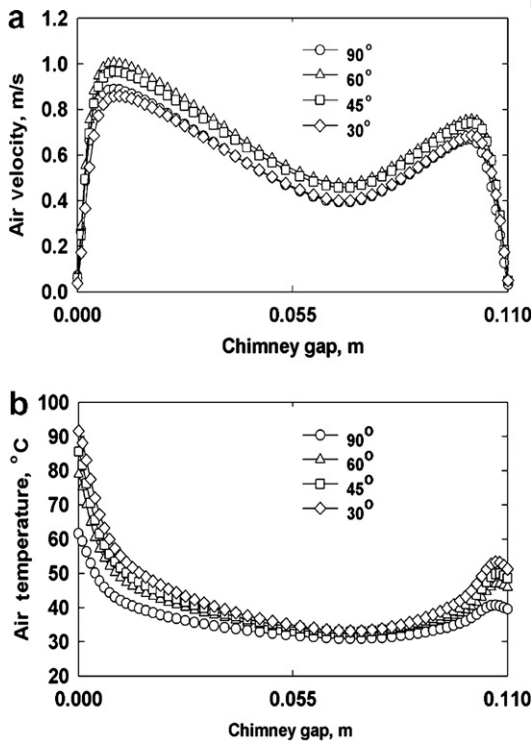


Fig. 4. Air velocity profile (a) and air temperature profile (b), across the chimney gap for different tilt angles for a chimney of 4m length as calculated by the CFD model (day = 196, $H = 23.1 \text{ MJ/m}^2$, $T_{\text{amb}} = 28.9 \text{ }^\circ\text{C}$).

In the above, Nu is the Nusselt number, Ra is the Rayleigh number, L is the length of the chimney and λ is the thermal conductivity of air. For inclinations between 30° and 75° , the heat transfer coefficient for the glass cover h_g (heated surface facing downwards) and the black wall h_{bw} (heated surface facing upwards) are calculated from the relations (VDI-Wärmeatlas, 1991):

$$Nu_g = \frac{h_g L}{\lambda} = 0.56 [Ra_g \sin(s)]^{1/4} \quad \text{for } 10^5 < Ra \sin(s) < 10^{11} \quad (39)$$

$$Nu_{bw} = \frac{h_{bw} L}{\lambda} = 0.56 [Ra_c \sin(s)]^{1/4} + 0.13 [Ra^{1/3} - Ra_c^{1/3}] \quad \text{for } 10^8 < Ra \sin(s) < 10^{11} \quad (40)$$

where Ra_c is a critical Rayleigh number that designates the transition between laminar and turbulent flow and which is given approximately by

$$\log(Ra_c) = 8.9 - 0.00178 \cdot (90 - s)^{1.82} \quad (41)$$

Eqs. (39) and (40) were originally obtained from experiments with inclinations below 75° . For this, for inclinations between 75° and 90° , cubic spline interpolation is employed to achieve smooth variation of coefficients with inclination.

In order to describe the average air velocity inside the chimney as a function of other system parameters, two different expressions have been tried. The first one is derived

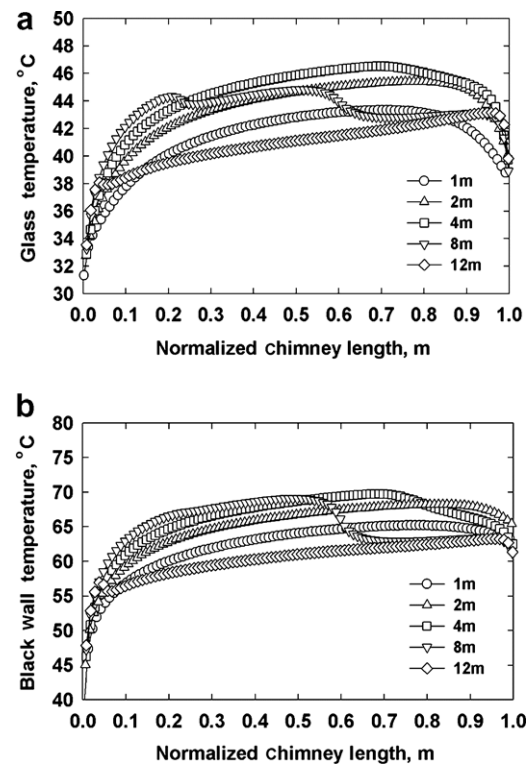


Fig. 5. Temperature of glazing (a) and absorber wall (b) along the normalized chimney length for different chimney lengths at the vertical position as calculated with the CFD model (day = 196, $H = 23.1 \text{ MJ/m}^2$, $T_{\text{amb}} = 28.9 \text{ }^\circ\text{C}$).

430 by assuming that the pressure head inside a tilted chimney
 431 counterbalances completely the pressure drop due to the
 432 wall friction and inlet and outlet pressure losses. For equal
 433 cross sectional areas at the inlet and outlet of the chimney
 434 and for small density differences along the chimney this
 435 yields:

$$437 \quad f \cdot \frac{L}{D_H} \cdot \frac{\rho_{\text{air}} v^2}{2} + k_{\text{in}} \cdot \frac{\rho_{\text{air}} v^2}{2} + k_{\text{out}} \cdot \frac{\rho_{\text{air}} v^2}{2} \\ = H_{\text{ch}} \cdot g \cdot \sin(s) \cdot (\rho_0 - \rho_{\text{air}}) \quad (42)$$

438 where D_H is the hydraulic diameter of the chimney defined
 439 as

$$441 \quad D_H = \frac{2 \cdot w \cdot d}{w + d} \quad (43)$$

442 w is the width of the chimney gap and d is the depth of the
 443 chimney gap. Also, k_{in} and k_{out} are the inlet and outlet
 444 pressure loss coefficients, H_{ch} is the height difference be-
 445 tween outlet and inlet of the chimney ($= L \cdot \sin(s)$) and f
 446 is the wall friction coefficient calculated (for turbulent flow)
 447 as

$$449 \quad f = \frac{0.316}{Re^{1/4}} \quad (44)$$

450 where Re is the apparent Reynolds number, defined as D_H
 451 $v \rho_{\text{air}} / \mu_{\text{air}}$. Combining the above yields:

$$454 \quad v = \left[\frac{2 \cdot L \cdot g (\sin(s))^2 (\rho_0 - \rho_{\text{air}})}{\left(f \cdot \frac{L}{D_H} + k_{\text{in}} + k_{\text{out}} \right) \cdot \rho_{\text{air}}} \right]^{1/2} \quad (45)$$

455 For a rectangular channel with both ends open and
 456 heated on one wall, Sandberg and Moshfegh (1998), pro-
 457 posed $k_{\text{in}} = 1.5$, $k_{\text{out}} = 1.0$ and $f = 0.056$.

458 The second expression that has been tried in the model
 459 was described by Bansal et al. (1993) and Andersen
 460 (1995). This is an empirical relation which uses the concept
 461 of a discharge coefficient to adjust the air velocity for the
 462 total flow resistances in the system (friction losses along
 463 the chimney wall, inlet and outlet pressure losses, etc).
 464 For a case of equal cross sectional areas at the inlet and
 465 outlet of the chimney this relation reduces to (T in Kelvin):
 466

$$468 \quad v_{\text{ave}} = C_d \cdot \frac{\rho(T_{\text{air}})}{\rho(T_0)} \cdot \left[\frac{L \cdot g \cdot (\sin(s))^2 \cdot (T_{\text{air}} - T_0)}{T_0} \right]^{1/2} \quad (46)$$

469 where C_d is the discharge coefficient which for thermal
 470 buoyant flows was proposed as 0.57 (Andersen, 1995).

471 2.2. CFD model

472 The commercial CFD code Fluent 6.1.18 is employed to
 473 simulate and check the heat transfer and fluid mechanics
 474 parts of the engineering model. For this, the CFD model
 475 uses as input data – apart from the chimney dimensions
 476 and material properties – the output data of the first two
 477 subroutines of the model, that is, the values of the total
 478 irradiation absorbed by the black wall and the glass cover.

479 Given the narrow geometry of our chimney (gap-to-
 480 length ratio 1:10), a 2D CFD model is considered adequate
 481 based on the assumption of uniform temperature distribu-
 482 tions across the chimney width. The employed geometrical
 483 domain has a variable length (1–12 m) as the first dimen-
 484 sion and a fixed gap depth (0.11 m) as the second one.
 485 The third dimension (width = 0.74 m) is used only for esti-
 486 mation of total flow rates. The computational grid is a pure
 487 map mesh with the cells clustered towards the black wall
 488 and the glass. The grid for the 1 m high chimney consists
 489 of 500 cells along the chimney and 55 cells across the gap
 490 (27,500 quad cells in total), with an average size of 2 mm.
 491 For the taller chimneys the grid size is increased propor-
 492 tionally in the length dimension to maintain the same spa-
 493 tial resolution.

494 Preliminary simulations showed that there are condi-
 495 tions where transition from laminar to turbulent flow
 496 occurs within the chimney and therefore, simulations are
 497 performed with both the laminar and turbulent models.
 498 For the latter, the shear-stress transport (SST) $k-\omega$ model
 499 with the transitional flows option active is used (Fluent
 500 user's guide, 2003), which is suitable for low Reynolds tur-
 501 bulent flows. This model combines the traditional two-
 502 layer turbulent zonal model with enhanced wall functions.
 503 A fine mesh close to the walls is created with $y^+ \approx 2$, to
 504 completely resolve the viscosity affected near-wall region.

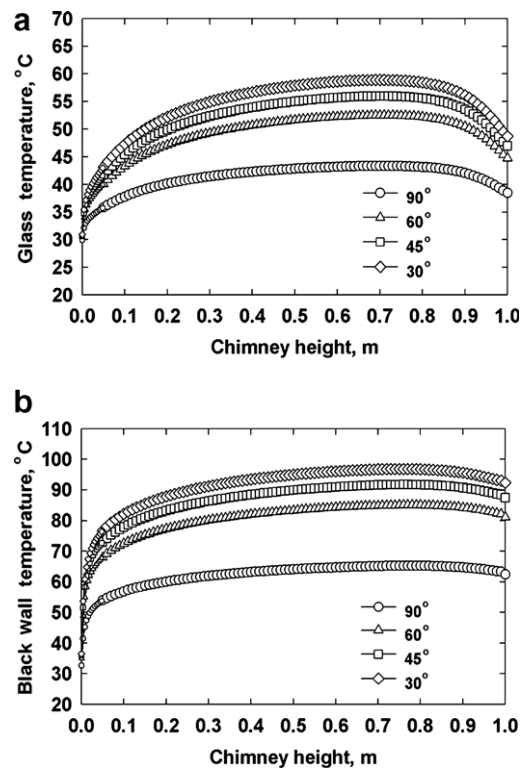


Fig. 6. Temperature of glazing (a) and absorber wall (b) along the normalized chimney length for different chimney tilt angles for a chimney of 1 m length as calculated with the CFD model (day = 196, $H = 23.1$ MJ/m², $T_{\text{amb}} = 28.9$ °C).

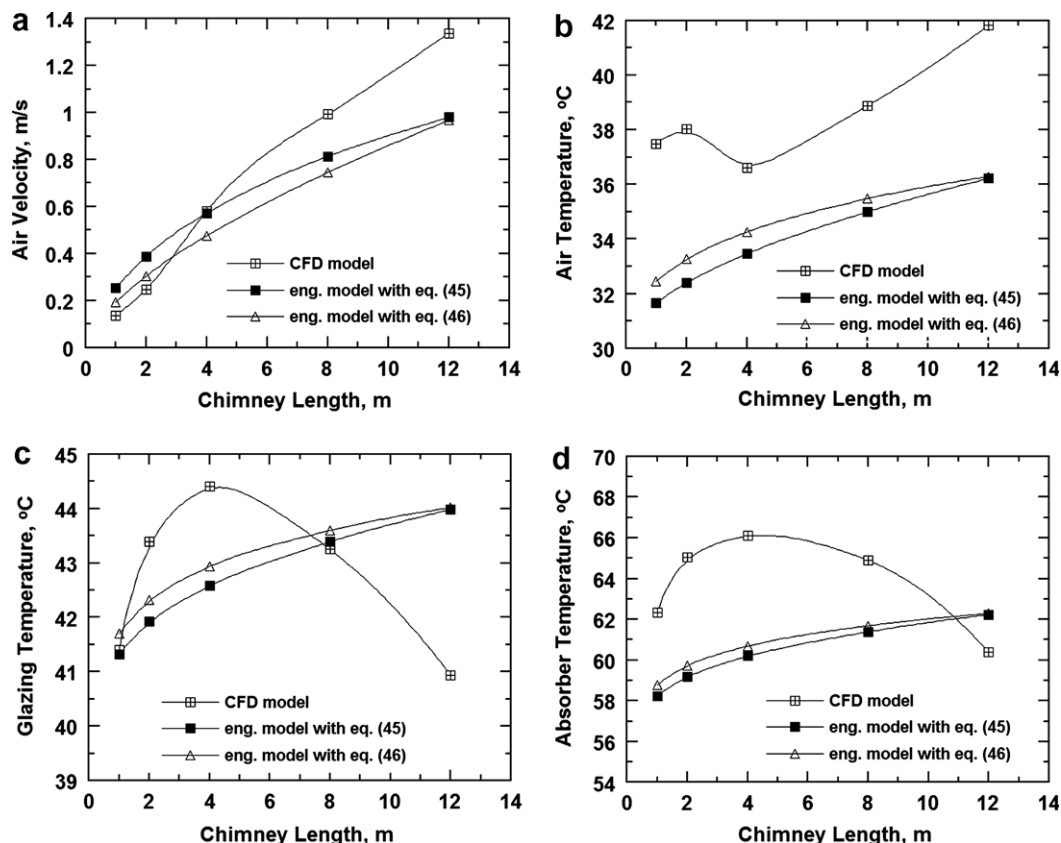


Fig. 7. Average air velocity (a), average air temperature (b), average glazing temperature (c) and average absorber temperature (d) versus chimney length at the vertical position as calculated by two versions of the engineering model and the CFD code (day = 196, $H = 23.1 \text{ MJ/m}^2$, $T_{\text{amb}} = 28.9 \text{ }^\circ\text{C}$).

505 The energy equation is employed to model the heat
 506 transfer phenomena with the Boussinesq approximation
 507 to hold for the density of air. Irradiation modeling is imple-
 508 mented using the Surface-to-Surface model (Fluent user's
 509 guide, 2003), which accounts for the irradiation exchange
 510 in an enclosure of gray-diffuse surfaces. The imposed
 511 boundary conditions for the two chimney walls, (glazing
 512 and absorbing black wall) are that they both have zero slip
 513 and internal emittance of 0.95.

514 3. Experiment

515 The experimental chimney duct has the shape of a nar-
 516 row parallelepiped with dimensions: 1 m height, 0.74 m
 517 width and 0.11 m gap. Black painted aluminum sheet
 518 (1.5 mm thick) is used for the construction of the rear
 519 and side walls of the chimney. These walls have high solar
 520 absorptance (~ 0.95) and low long wave emittance (~ 0.05)
 521 (Garg, 1987). A 5 cm thick fiberglass layer ($\lambda = 0.045 \text{ W/}$
 522 m K) is the outside insulation material of these walls. The
 523 chimney's front side (glazing) is a commercial glass,
 524 3 mm thick. The chimney glazing has a south orientation
 525 at all times.

526 In order the chimney to stand at various inclinations, it
 527 is mantled onto a short (0.5 m) metallic trapezoid equip-
 528 ped with special fittings that allow the chimney to lie at different
 529 tilt positions. Special care is given to make the chimney

530 light enough so that it can be stably supported by the trap-
 531 ezoid when tilted and so permit easy handling of measuring
 532 probes. Even so, for slopes less than 45° it was difficult to
 533 hold the chimney firmly.

534 Along the two vertical narrow side walls of the paralle-
 535 piped's section ($1 \times 0.11 \text{ m}$), five holes are drilled to facilit-
 536 ate the insertion of measuring probes at distances 0.14 m,
 537 0.34 m, 0.54 m, 0.75 m and 0.89 m from the bottom of the
 538 chimney, respectively. Special contact-type thermocouples
 539 (K type, OMEGA Inc.) are employed to measure the sur-
 540 face temperature of the glazing and the black wall at three
 541 positions across the chimney width (left, center, right) to
 542 check for 3D effects. From the recorded data, average val-
 543 ues are presented from those three positions since the var-
 544 iance ($= \text{SD/average}$) is less than 0.05. Fig. 1b shows a
 545 photo of the constructed solar chimney where the five mea-
 546 suring stations along the vertical side wall are indicated.

547 Efforts have been made to measure the velocity of the air
 548 in the chimney with a hot-wire anemometer probe fur-
 549 nished with sensitive temperature sensors (DO 2003,
 550 DELTA OHM). Unfortunately, due to the low height of
 551 the chimney, the measured velocities were always below
 552 0.2 m/s. For such low velocities – although within the mea-
 553 suring range of the anemometer – the readings were very
 554 unstable perhaps due to minor atmospheric disturbances.
 555 So, comparisons with theoretical predictions are based on
 556 temperature measurements. This shortcoming is partly alle-

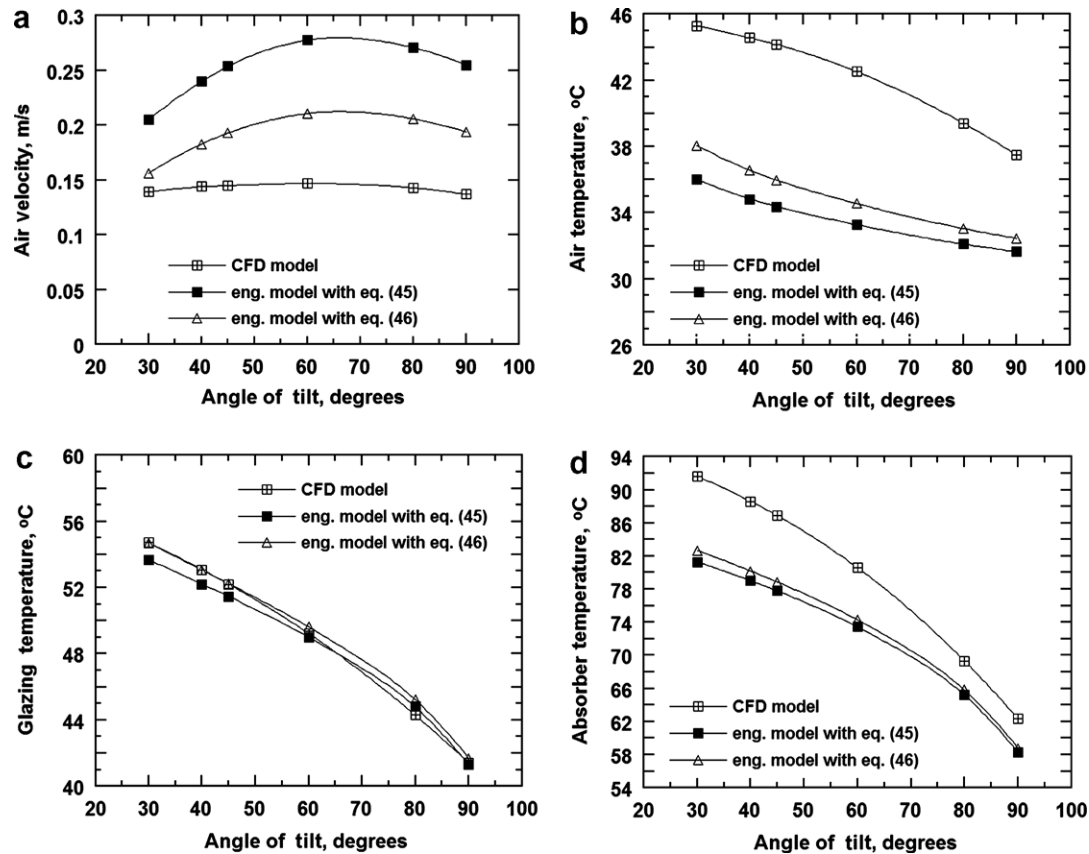


Fig. 8. Average air velocity (a), average air temperature (b), average glazing temperature (c) and average absorber temperature (d) versus chimney tilt for a chimney of 1 m length as calculated by two versions of the engineering model and the CFD code (day = 196, $H = 23.1 \text{ MJ/m}^2$, $T_{\text{amb}} = 28.9 \text{ }^\circ\text{C}$).

557 viated by the fact that with such a low height (i.e., light-
558 weight) chimney it was possible to use it at different inclina-
559 tions, an issue essential for this work.

560 Total horizontal irradiation data are collected and inte-
561 grated over 10 min intervals, for the period of the exper-
562 iments with an Eppley Precision Pyranometer (model
563 PSP). The experiments are performed in Serres, Greece
564 (latitude $41^\circ 07'$, longitude $23^\circ 34'$, altitude 32 m).

565 4. Results and discussion

566 4.1. CFD parametric study

567 It is illustrative to display first the CFD calculations in
568 order to appreciate the velocity and temperature profiles
569 in the chimney and their variation with respect to height
570 and tilt. Due to space limitations only simulations at a
571 summer day are presented: day 196 (mid July), monthly
572 average daily total irradiation on a horizontal plane
573 23.1 MJ/m^2 and monthly average daily ambient tempera-
574 ture $28.9 \text{ }^\circ\text{C}$. These data are taken for the city of Serres
575 from ELOT (1991).

576 Fig. 2a shows the air velocity profile across the chimney
577 gap at the exit of a vertical chimney, with chimney length
578 as a parameter. The shape of the velocity profiles for the
579 two smaller lengths (1 and 2 m) are typical of non-interact-

ing boundary layers flowing past the absorber wall (gap 580
position = 0) and the glazing (gap position = 0.11), respec- 581
tively. Two local maxima are observed near these walls (the 582
higher for the hotter absorber wall) whereas at the centre of 583
the chimney the velocity is close to zero. So, it is not so 584
strange that we were not able to measure significant air 585
velocities in our 1 m chimney. The situation changes for 586
higher chimneys where the two boundary layers start to 587
interact leading to less pronounced local maxima and a 588
smoother velocity front with appreciable velocities at the 589
center of the chimney. The overall air velocity (and there- 590
fore air flow rate) increases significantly with chimney 591
length due to the higher pressure head but also higher dif- 592
ference between inside air temperature and ambient tempera- 593
ture. Above 4 m, full pipe flow prevails which, yet, is 594
not symmetrical across the gap. Inspection of the CFD 595
results (not shown due to space limitations) shows a transi- 596
tion from laminar to turbulent flow for higher than 597
 $\sim 3 \text{ m}$ chimneys. 598

599 Fig. 2b displays the corresponding mass-weighted –
“cup-mixing” – air temperature profiles. Mass-weighted 600
temperature values depict better the energy content of air 601
which affects the flow rate. As expected, the higher air tem- 602
peratures are near the black absorber wall which seems to 603
be the main heat supplier of the system. Again, for 1 m and 604
2 m chimneys the two boundary layers hardly sense each 605

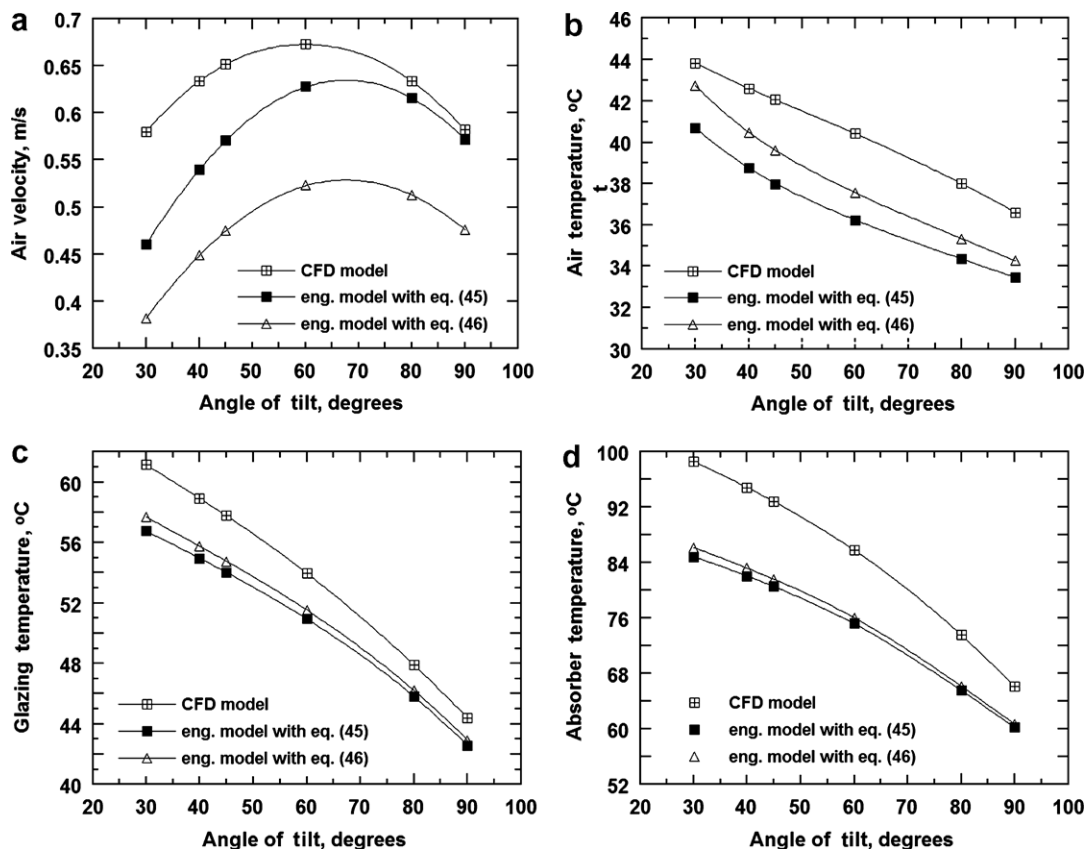


Fig. 9. Average air velocity (a), average air temperature (b), average glazing temperature (c) and average absorber temperature (d) versus chimney tilt for a chimney of 4 m length as calculated by two versions of the engineering model and the CFD code (day = 196, $H = 23.1 \text{ MJ/m}^2$, $T_{\text{amb}} = 28.9 \text{ }^\circ\text{C}$).

606 other; the temperatures at the center of the gap being very
 607 close to the incoming ambient temperature. This, changes
 608 drastically for chimneys above 4 m. For the latter, an inter-
 609 esting change of the slope of the profiles occurs near the
 610 glazing as a result of temperature mass-weighting.

611 Figs. 3 and 4 show the influence of the tilt position on
 612 (a) air velocity and (b) mass-weighted air temperature
 613 across the chimney gap for chimney lengths 1 m and 4 m,
 614 respectively. The main features of both the velocity and
 615 temperature profiles are essentially those described in
 616 Fig. 2 and do not seem to vary with tilt. For both chim-
 617 neys, it is clear that the higher velocities are achieved at
 618 60° whereas the higher temperatures at 30°. In addition,
 619 the air temperature in contact with the walls for the vertical
 620 chimney is appreciably lower than the values for the other
 621 angles but this is not so for the velocity. Both the above
 622 findings manifest a different influence of tilt on heat trans-
 623 fer and fluid flow in the chimney with the consequence that
 624 the maximum energy uptake not to coincide with the max-
 625 imum air flow rate.

626 The influence of chimney length on (a) the glazing tem-
 627 perature and (b) the absorber temperature is shown in
 628 Fig. 5 for an inclination of 90°. Normalization in the length
 629 scale is performed by division with the total chimney
 630 length. Qualitatively speaking, the two walls exhibit similar
 631 trends. However, the absorber is always warmer than the

632 glazing at the same length. Both walls are heated up signifi-
 633 cantly within a very short distance from the inlet of the
 634 chimney since there velocities are low and so energy cannot
 635 be promptly transferred to the air stream. A bit upstream
 636 where the walls are already warm, their temperature
 637 increases more gradually because both the air velocity
 638 and the temperature difference ($T_{\text{wall}} - T_{\text{air}}$) driving the
 639 heat transfer towards the air become significant. Near the
 640 top of the chimney, irradiation losses come into play and
 641 reduce the temperature of the walls. It is interesting that
 642 for chimneys between 1 and 4 m length, the local tempera-
 643 ture of the walls increases with length. On the contrary, for
 644 higher chimneys the local temperature of the walls
 645 decreases with length. This may be attributed to full pipe
 646 turbulent flow that starts to develop for chimneys above
 647 ~3 m. When this happens, the heat transfer coefficient
 648 increases and so the walls are cooled down. The same tran-
 649 sition phenomena most probably explain also the stepwise
 650 drop of temperature midway the 8 m chimney. For even
 651 higher chimneys, e.g. 12 m, the wall temperatures increase
 652 almost linearly with height indicating a pretty constant tur-
 653 bulent field.

654 Fig. 6 illustrates the influence of the tilt angle on (a) the
 655 glazing temperature and (b) the absorber temperature for a
 656 chimney of 1 m length. As can be seen, the local tempera-
 657 tures get higher as the tilt gets lower, for both walls. This is

658 qualitatively what has been also observed in Fig. 3b regard- 711
 659 ing the air temperature and demonstrates that there is a 712
 660 direct relationship between the thermal condition of the 713
 661 walls and that of air. If one further considers Fig. 3a, it 714
 662 is apparent that in solar chimneys the tilt for maximum 715
 663 absorbed irradiation does not coincide with the tilt for 716
 664 maximum air flow. 717

665 4.2. Comparison between CFD and engineering models 719

666 Fig. 7a–d compares CFD predictions with predictions 720
 667 from the engineering model, as a function of chimney 721
 668 length for a vertical orientation of the chimney. Predictions 722
 669 refer to average air velocity and air temperature in the 723
 670 chimney as well as average glazing temperature and absor- 724
 671 ber temperature. Two series of model predictions are pre- 725
 672 sented; one based on Eq. (45) and the other on Eq. (46) 726
 673 for the estimation of air velocity in the chimney. Results 727
 674 only for day 196 (mid July) are presented since this proved 728
 675 to be the most stringent period for comparisons with the 729
 676 largest deviations between models. In all four plots, it is 730
 677 apparent that the two versions of the engineering model 731
 678 give comparable results. Yet, they are different from the 732
 679 CFD results. Regarding air velocity, CFD data are lower 733
 680 than the engineering model data for chimneys less than
 681 2 m but the situation reverses for chimneys above 4 m.
 682 Air temperatures predicted by the engineering model are
 683 below the values predicted by the CFD code for all the
 684 examined lengths. Interestingly, CFD results show a non-
 685 monotonous sigmoid behavior with a kink point around
 686 4 m. This is most likely due to the prevailing turbulent con-
 687 ditions for chimneys longer than 4 m. A non-monotonous
 688 behavior is also observed in the CFD predictions of the
 689 glazing and absorber temperatures with a peak value again
 690 close to 4 m. The latter means that for chimneys taller than
 691 4 meters heat transfer from the walls to the flowing air is
 692 drastically enhanced, indicating once more turbulent flow
 693 conditions.

694 Figs. 8a–d and 9a–d show the dependence of all model 734
 695 predictions on the angle of the tilt for chimney lengths 735
 696 1 m and 4 m, respectively. Calculations are again for day 736
 697 198 (mid-July) where comparisons among models are less 737
 698 favorable. Despite the deviations among models in the pre- 738
 699 dicted values of air velocity, air temperature, glazing tem- 739
 700 perature and absorber temperature, there is a good 740
 701 agreement on the optimum tilt that yields maximum air 741
 702 velocity: The engineering model predicts an optimum tilt 742
 703 around 65° whereas the CFD code around 60°. This result 743
 704 has great significance as it lends support in the use of the 744
 705 simpler engineering model for preliminary design purposes 745
 706 and for comparisons between cases. 746

707 4.3. Comparison between predictions and experiments 747

708 Next, the CFD and the engineering model predictions 748
 709 are compared against experimental measurements. The 749
 710 days for conducting the experiments were carefully selected 750

for wind speed to be less than 0.5 m/s. Runs were per-
 formed at days 305, 306 and 307 (beginning of November).
 The values of total horizontal irradiation and ambient tem-
 perature mentioned in the Figure captions are those mea-
 sured on the spot and used as inputs to the models. It
 must be stressed in advance that for November the devia-
 tions between CFD and engineering model predictions
 are much less than for July (worst case).

Fig. 10a compares the predicted glazing and absorber
 temperatures to measured values for a vertical position of
 the chimney. Error bars denote the standard deviation of
 measurements. During the measuring period the ambient
 temperature was not constant so two series of CFD data
 were calculated based on two different values for the ambi-
 ent temperature. The first one is the average temperature
 and the second one the median temperature of the measur-
 ing period. As can be seen, the experimental data agree rea-
 sonably well with predictions. Fig. 10b displays
 comparisons regarding the average air temperature. There
 is again a fair agreement between data and predictions.
 This is even more so if one considers that measurements
 may be a bit higher than in reality due to the irradiation
 absorbed by the finite size measuring probe (part of the

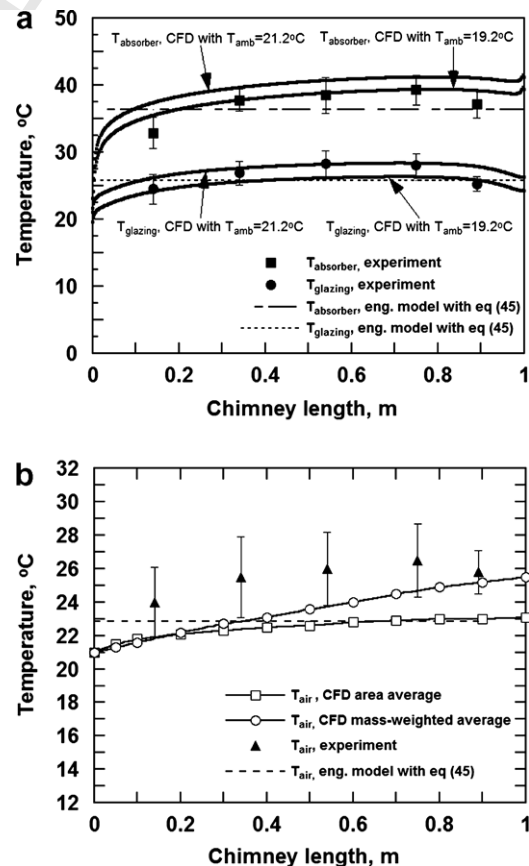


Fig. 10. Comparison between the engineering model predictions against CFD and experimental results as regards (a) the temperatures of the glazing and the absorber and (b) the air temperature along the chimney length. Plot (a): day = 307, $H = 8.12 \text{ MJ/m}^2$, median $T_{amb} = 19.2^\circ\text{C}$, average $T_{amb} = 21.2^\circ\text{C}$. Plot (b): day = 307, $H = 8.12 \text{ MJ/m}^2$, average $T_{amb} = 21.2^\circ\text{C}$.

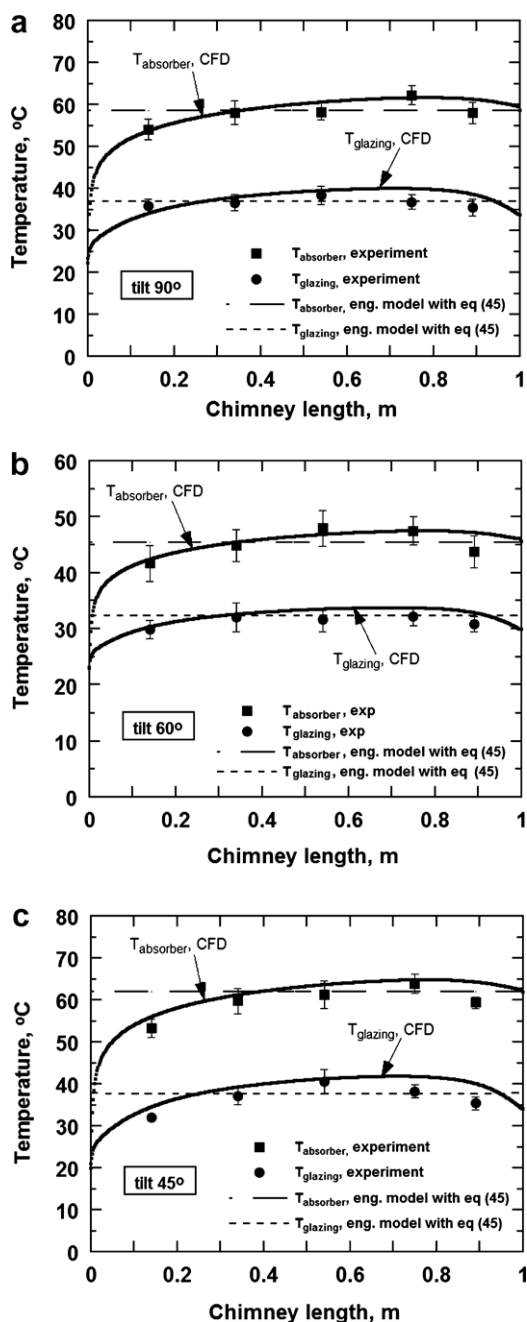


Fig. 11. Comparison between the engineering model predictions against CFD and experimental results as regards the temperatures of the glazing and the absorber along the chimney length (a) for 90°, (b) 60° and (c) 45° angle of tilt. Plot (a): day = 305, $H = 9.70 \text{ MJ/m}^2$, $T_{\text{amb}} = 21.7^\circ\text{C}$. Plot (b): day = 305, $H = 9.05 \text{ MJ/m}^2$, $T_{\text{amb}} = 19.1^\circ\text{C}$. Plot (c): day = 306, $H = 9.90 \text{ MJ/m}^2$, $T_{\text{amb}} = 23.1^\circ\text{C}$.

hot wire probe). Fig. 11a–c shows comparisons for the chimney placed on the trapezoid base and fixed at three different inclinations. Again the agreement between predictions and measurements is good.

4.4. Chimney tilt for maximum air flow

Calculations with the engineering model (using Eq. (45)) for the different months of the year to identify the optimum

tilt yielding maximum air flow are presented next, Fig. 12a. The input values of monthly average daily total irradiation on a horizontal plane and monthly average daily ambient temperature, are taken from ELOT (1991). The corresponding maximum velocity values are also displayed to allow appraisal of changes throughout the year. For comparison, Fig. 12b shows the tilt that yields maximum absorbed irradiation along with the corresponding irradiation values on the horizontal plane.

Clearly, air velocity and total irradiation exhibit similar trends receiving their lower values during summer months. However, the angles themselves are very different. So, for maximum air flow the chimney tilt varies in a rather narrow range between 65° and 76° whereas for maximum irradiation it varies between 12° and 44°. Furthermore, the variation of irradiation values throughout the year is much larger (on a percentage basis) than the variation of velocity values. In the relevant work of Prasad and Chandra (1990), conducted for a location in India, qualitatively similar trends were observed but the range of the angles was different: between 53° and 76° for maximum air flow and between 0° and 55° for maximum irradiation.

The question now arises on what is the best choice for the tilt if the chimney is to be fixed at one and only inclina-

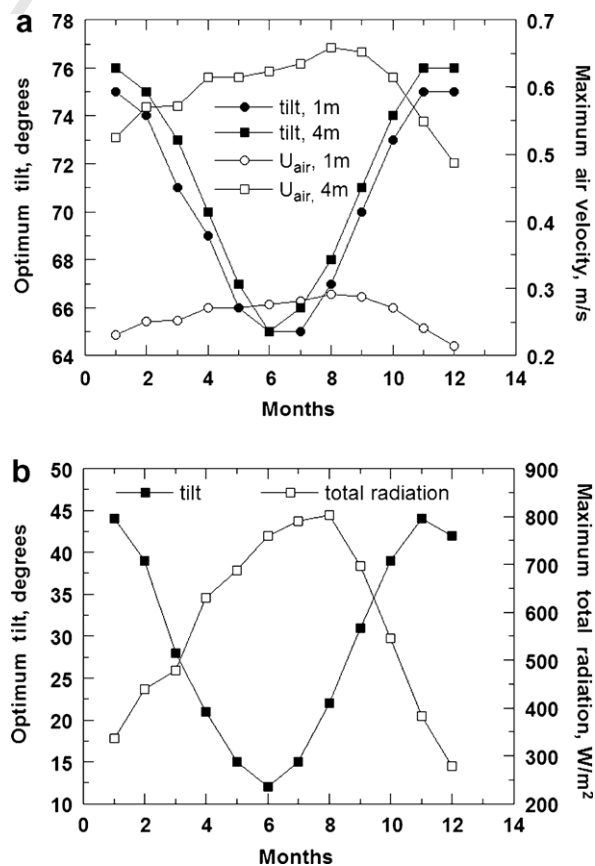


Fig. 12. (a) Optimum tilt and corresponding maximum air velocity (for a 1 m and a 4 m chimney) and (b) optimum tilt and corresponding maximum total irradiation (for any chimney length) versus month of the year as calculated by the engineering model.

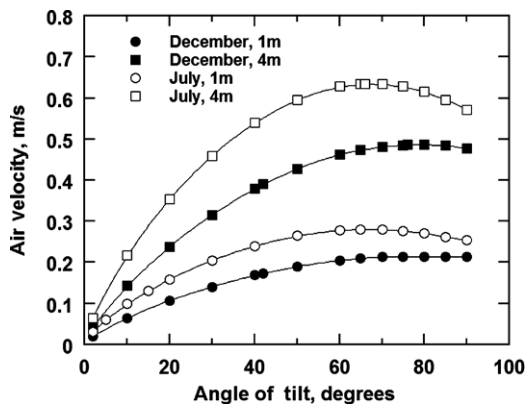


Fig. 13. Average air velocity versus chimney tilt for a 1 m and a 4 m chimney as calculated by the engineering model for the mid day of December and July.

Acknowledgements

The project is co-funded by the European Social Fund and National Resources – (EPEAEK-II) ARHIMIDIS. The authors are indebted to Mr. N. Vallous for his editorial work.

References

- Afonso, C., Oliveira, A., 2000. Solar chimneys: simulation and experiment. *Energy and Buildings* 32, 71–79.
- Andersen, K.T., 1995. Theoretical considerations on natural ventilation by thermal buoyancy. *ASHRAE Transactions* 101 (2), 1103–1117.
- Awbi, H.B., Gan, G., 1992. Simulation of solar-induced ventilation. In: *Proceedings of the Second World Renewable Energy Congress (WREC '92)*, vol. 4, Reading, UK, pp. 2016–2030.
- Badescu, V., 2002. 3D approximation for solar diffuse irradiance on tilted surfaces. *Renewable Energy* 26, 221–233.
- Bansal, N.K., Mathur, R., Bhandari, M.S., 1993. Solar chimney for enhanced stack ventilation. *Building and Environment* 28, 373–377.
- Bansal, N.K., Mathur, J., Mathur, S., Jain, M., 2005. Modeling of window-sized solar chimneys for ventilation. *Building and Environment* 40, 1302–1308.
- Bouchair, A., 1994. Solar chimney for promoting cooling and ventilation in Southern Algeria. *Building Service Engineering Research Technology* 15 (2), 81–93.
- Bouchair, A., Fitzgerald, D., 1988. The optimum azimuth for a solar chimney in hot climates. *Energy and Buildings* 12, 135–140.
- Chen, Z.D., Bandopadhyay, P., Halldorsson, J., Byrjalsen, C., Heiselberg, P., Li, Y., 2003. An experimental investigation of a solar chimney model with uniform wall heat flux. *Building and Environment* 38, 893–906.
- Dai, Y.J., Sumathy, K., Wang, R.Z., Li, Y.G., 2003. Enhancement of natural ventilation in a solar house with a solar chimney and a solid adsorption cooling cavity. *Solar Energy* 74, 65–75.
- Das, S.K., Kumar, Y., 1989. Design and performance of a solar dryer with vertical collector chimney suitable for rural application. *Energy Conversion Management* 29 (2), 129–135.
- Ding, W., Minegishi, Y., Hasemi, Y., Yamada, T., 2004. Smoke control based on a solar-assisted natural ventilation system. *Building and Environment* 39, 775–782.
- Ding, W., Hasemi, Y., Yamada, T., 2005. Natural ventilation performance of a double-skin façade with a solar chimney. *Energy and Buildings* 37, 411–418.
- Duffie, J.A., Beckman, W.A., 1991. *Solar Engineering of Thermal Processes*, second ed. Wiley-Interscience, New York, pp. 3–146.
- Ekechukwu, O.V., Norton, B., 1995. Design and measured performance of a solar chimney for natural circulation solar energy dryers. *Journal of Solar Energy Engineering* 118, 69–71.
- ELOT, 1991. Greek Bureau of Standards No. 1291.
- Fluent user's guide, 2003. Fluent Inc.
- Gan, G., 1998. A parametric study of Trombe walls for passive cooling of buildings. *Energy and Buildings* 27, 37–43.
- Gan, G., Riffat, S.B., 1998. A numerical study of solar chimney for natural ventilation of buildings with heat recovery. *Applied Thermal Engineering* 18, 1171–1187.
- Garg, H.P., 1987. Solar food drying. In: *Advances in Solar Energy Technology Collection and Storage Systems*, vol. 1. D. Reidel Publishing Co., Dordrecht, pp. 1–123.
- Hamdy, I.F., Fikry, M.A., 1998. Passive solar ventilation. *Renewable Energy* 14, 381–386.
- Heras, M.R., Jiménez, M.J., San Isidro, M.J., Zarzalejo, L.F., Pérez, M., 2005. Energetic analysis of a passive solar design, incorporated in a courtyard after refurbishment, using an innovative cover component based in a sawtooth roof concept. *Solar Energy* 78, 85–96.

tion throughout the year. To help answer this, Fig. 13 displays the air velocity versus the tilt for a 1 m and a 4 m chimney and for the midday of December and July. Evidently, for winter applications the slight increase (~1%) in air velocity by using the optimum tilt (as compared to a vertical chimney) is not worth it against concerns about the stability of the construction. However, during summer months the gain in air velocity for the optimum tilt is around 10% and decisions must be made more carefully.

5. Conclusion

A composite engineering model is developed that estimates the tilt of a solar chimney that yields the largest natural air flow through it. The model starts by calculating the solar energy absorbed by the solar chimney of varying tilt and height for a given time (day of the year, hour) and place (latitude). The monthly average daily value of total irradiance and the ambient temperature are required as inputs to the code along with some information on the dimensions and properties of the construction materials (absorber, glazing, insulation). The outputs of the model are the velocity and temperature of the air inside the chimney and the temperatures of the glazing and the black painted absorber, as a function of tilt and height. Comparisons of the model predictions with CFD results for a broad range of chimney lengths (1–12 m) and tilts (30–90°) delineates the usefulness of the model but marks also its limitations. Moreover, model predictions are in satisfactory accord with experimental measurements from a 1 m chimney operated at different inclinations. The reasonable agreement between model predictions with CFD and experimental results encourages the use of the engineering model as a tool for evaluating design parameters and for comparative studies.

6. Uncited reference

Ding et al. (2005).

- 863 Jiang, Y., Chen, Q., 2003. Buoyancy-driven single-sided natural ventila- 888
864 tion in buildings with large openings. *International Journal of Heat* 889
865 *and Mass Transfer* 46, 973–988. 890
- 866 Karapantsios, T.D., Hatzimoisiadis, K.A., Balouktsis, A.I., 1999. Esti- 891
867 mation of total atmospheric pollution using global irradiation data: 892
868 introduction of a novel clear day selection methodology. *Renewable* 893
869 *Energy* 17, 169–181. 894
- 870 Kazansky, S., Dubovsky, V., Ziskind, G., Letan, R., 2003. Chimney- 895
871 enhanced natural convection from a vertical plate: experiments and 896
872 numerical calculations. *International Journal of Heat and Mass* 897
873 *Transfer* 46, 497–512. 898
- 874 Khedari, J., Boonsri, B., Hirunlabh, J., 2000. Ventilation impact of a solar 899
875 chimney on indoor temperature fluctuation and air change in a school 900
876 building. *Energy and Buildings* 32, 89–93. 901
- 877 Khedari, J., Rachapradit, N., Hirunlabh, J., 2003. Field study of 902
878 performance of solar chimney with air-conditioned building. *Energy* 903
879 28, 1099–1114. 904
- 880 Kumar, S., Sinha, S., Kumar, N., 1998. Experimental investigation of a 905
881 solar chimney assisted bioclimatic architecture. *Energy Conversion* 906
882 *Management* 39, 441–444. 907
- 883 Liu, B.Y.H., Jordan, R.C., 1963. The long term average performance of 908
884 flat plate solar energy collectors. *Solar Energy* 7, 53–74. 909
- 885 Moshfegh, B., Sandberg, M., 1999. Flow and heat transfer in the air gap 910
886 behind photovoltaic panels. *International Journal of Renewable and* 911
887 *Sustainable Energy Reviews* 2, 287–301. 912
913
- Ong, K.S., Chow, C.C., 2003. Performance of a solar chimney. *Solar* 888
Energy 74, 1–17. 889
- Prasad, M., Chandra, K.S., 1990. Optimum tilt of solar collector for 890
maximum natural flow. *Energy Conversion Management* 30, 369– 891
379. 892
- Raman, P., Mande, S., Kishore, V.V.N., 2001. A passive solar system for 893
thermal comfort conditioning of buildings in composite climates. *Solar* 894
Energy 70, 319–329. 895
- Rodrigues, A.M., Canha da Piedade, A., Lahellec, A., Grandpeix, J.Y., 896
2000. Modelling natural convection in a heated vertical channel for 897
room ventilation. *Building and Environment* 35, 455–469. 898
- Sánchez, M.M., Lucas, M., Martínez, P., Sánchez, A., Viedma, A., 2003. 899
Climatic solar roof: an ecological alternative to heat dissipation in 900
buildings. *Solar energy* 73, 419–432. 901
- Sandberg, M., Moshfegh, B., 1998. Ventilated-solar roof air flow and heat 902
transfer investigation. *Renewable Energy* 15, 287–292. 903
- Sukhatme, S.P., 1984. *Solar Energy: Principles of Thermal Collection and* 904
Storage. McGraw-Hill, New Delhi, pp. 58–82. 905
- VDI-Wärmeatlas, 1991. VDI-Verlag GmbH, Dusseldorf, pp. Db15-Db28, 906
Fc1-Fc3, Fd1-Fd4. 907
- Vlachos, N.A., Karapantsios, T.D., Balouktsis, A.I., Chassapis, D., 2002. 908
Design and testing of a new solar tray dryer. *Drying Technology* 20, 909
1243–1271. 910
- Ziskind, G., Dubovsky, V., Letan, R., 2002. Ventilation by natural 911
convection of a one-story building. *Energy and Buildings* 34, 91–102. 912
913